

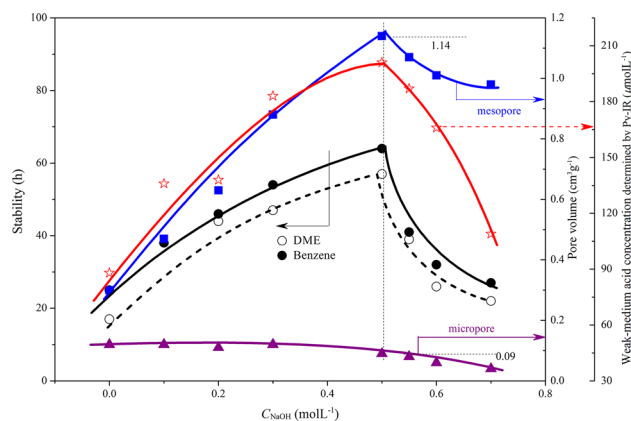
Effect of Desilication on the Performance of Hierarchical ZSM-11 Catalysts for Alkylation of Benzene with Dimethyl Ether

Hui Liu^{1,2} · Shenglin Liu¹ · Sujuan Xie¹ · Chao Song^{1,2} · Wenjie Xin¹ · Longya Xu¹

Received: 9 April 2015 / Accepted: 12 July 2015
© Springer Science+Business Media New York 2015

Abstract Hierarchical ZSM-11 zeolites (Z-xat) were prepared by treating the pristine ZSM-11 zeolite in a solution of NaOH with different concentrations (C_{NaOH}). It was found the porosity and acidity (concentration, strength, distribution and accessibility factor of Brønsted and Lewis acid sites) of modified ZSM-11 zeolite changed obviously with C_{NaOH} . When used for alkylation of benzene with dimethyl ether, the modified Z-xat exhibited better reaction stability than the unmodified HZSM-11 zeolite. Typically, the reaction stability of Z-xat zeolite catalysts was directly related to the mesopore volume, besides the weak-medium acid concentrations determined by Py-IR technique.

Graphical Abstract



Keywords Hierarchical ZSM-11 · Alkaline treatment · Brønsted and Lewis acid sites · Accessibility factor · Alkylation of benzene with DME

1 Introduction

ZSM-11 zeolite (MEL topology) possesses two straight intersecting channels, which is similar with the ZSM-5 (MFI topology) consisting of intersectional straight and sinusoidal channels [1–3]. In spite of the similarity, few studies on ZSM-11 have been reported, compared with the widely studied ZSM-5 zeolite [4].

As far as the porosity of zeolite, the sole presence micropores may inevitably impose diffusion limitations or confinement effects [5] on the shape-selective reactions and adsorption rates. Enormous alternative strategies have been attempted to circumvent this problem [6, 7], and

Electronic supplementary material The online version of this article (doi:10.1007/s10562-015-1589-1) contains supplementary material, which is available to authorized users.

✉ Longya Xu
lyxu@dicp.ac.cn; liuhui@dicp.ac.cn

¹ State Key Laboratory of Catalysis, Dalian Institute of Chemical Physics, Chinese Academy of Sciences, Dalian 116023, Liaoning, China

² University of Chinese Academy of Sciences, Beijing 100049, China

desilication in alkaline aqueous solution has become the most promising method to introduce hierarchical micro-mesoporous system [8–11], due to the cheap and facile operation and efficient mesopores production.

Except for the porosity, acidity is another significant feature for zeolite, due to its influence on catalytic and reaction performance on catalysts [12, 13]. Zeolites contain many different kinds of acid sites in terms of their types and strengths, as well as their locations in the zeolite pore system. In addition to conventionally used NH_3 -TPD and pyridine-adsorption IR techniques, recently the acid sites located on the external surface have been investigated with the IR technique of lutidine and collidine [14–16] and 2,6-di-tert-butylpyridine [16–18] adsorption, however, these studies were only limited to the Brønsted acid sites. And only non-quantitative accessibility of Lewis acid sites on external surface was obtained by indirect method [19].

Fortunately, the IR technique of pivalonitrile adsorption (Pn-IR) has been developed and used to characterize both Brønsted and Lewis acid sites located on external surfaces and in pore mouths [20–22]. However, such a kind of IR technique was only reported for HZSM-5 zeolites, and no any work for other kinds of zeolites has been reported till now.

ZSM-11 zeolite attracts more and more attention in many fields recently [1–3]. Nevertheless, little information is available regarding the effect of ZSM-11 by alkaline treatment (NaOH). Moreover, how the NaOH concentration (denoted as C_{NaOH}) exactly affects the mesopores production and acidic properties for ZSM-11 zeolite are reported rarely up to now. Despite plenty of acidity and porosity investigation for different hierarchical zeolites [16, 23, 24], there is little systematic report about the types, strength, distribution (B/L ratio) and accessibility factor (AF) of different acid sites variation with the concentration of alkaline.

Recently, the alkylation of benzene has been received much more interest since the aromatic hydrocarbon products are highly needed by the market around the world. In spite of this situation, alkylation of benzene with dimethyl ether (DME) has been reported only by Széchenyi et al. [25]. Recently, we investigated the alkylation of benzene with DME over Zn loaded [26] and AIPO bounded [3] ZSM-11 zeolite catalysts, in which we explored the effect of Zn and P modification on the zeolite catalytic performance. As an extension, this work systematically studied the pristine ZSM-11 zeolite materials treated with NaOH solution with different concentrations.

The changes of structural properties and acidities for the as modified materials were characterized by many techniques, such as X-ray diffraction, X-ray fluorescence, N_2 and Benzene adsorption–desorption isotherms measurements, scanning and transmission electron microscopy,

ammonia temperature-programmed desorption as well as pyridine-adsorption IR and Pn-IR measurements. The acid sites located on external surfaces and in pore mouths monitored by Pn-IR technique and the corresponding accessibility factor were first reported for the modified ZSM-11 zeolites. The obtained hierarchical ZSM-11 zeolites were tested in the alkylation of benzene with DME. The results suggested that the alkaline treatment was helpful for improving the reaction performance of the desilicated ZSM-11 catalyst zeolite. Besides, the difference in the reaction stability was relevant to the porosity and acidity of the as prepared hierarchical ZSM-11 zeolites.

2 Experimental

2.1 Synthesis of ZSM-11 Zeolite and Treated with Pure NaOH Solution

ZSM-11 of Si/Al₂ of 53 (particle size of 300–400 nm) was synthesized in laboratory based on our previous work [1]. Prior to the treatment, the as-synthesized zeolite was calcined in static air at 540 °C for 4 h in order to remove the template. The calcined sample was desilicated by NaOH solution as follows. ZSM-11 zeolite powder of 8 g was treated in aqueous NaOH solutions with the concentration ranging from 0.1 to 1.0 M of 280 mL under stirring at 75 °C for 15 min. The suspensions were then quenched in cold water and filtered, and the isolated solids were washed with deionized water until it had a neutral PH. Then, all the samples were converted to the protonic form by conventional ion exchange in aqueous NH_4NO_3 solution (0.8 M, 80 °C, 1 h, 20 cm³ per gram of zeolite for 3 times), followed by calcination (air condition, 510 °C, 3 h). The name of the resultant samples was denoted as Z-*x*at, where “*x*” related to the concentration of NaOH solution applied. Accordingly, the unmodified sample was denoted as HZSM-11.

2.2 Catalyst Characterization

X-ray diffraction (XRD) patterns were recorded on an X'Pert PRO X-ray diffractometer using Cu K α radiation (40 kV, 40 mA), with a scanning range of 2θ from 5° to 50° at a scanning rate of 10° min⁻¹. The relative crystallinity is calculated based on the relative intensities of the reflection at $2\theta = 7.9 \pm 0.1^\circ$, $8.8 \pm 0.1^\circ$, $23.0 \pm 0.1^\circ$, $23.8 \pm 0.1^\circ$ and $45.0 \pm 0.1^\circ$, taking the crystallinity of the pristine HZSM-11 zeolite to be 100 %.

X-ray fluorescence (XRF) experiments were conducted on a Philips Magix 601X X-ray fluorescence spectrometer, and IQ+ quantitative software package was employed for the analysis.

N₂ adsorption–desorption isotherms were performed on Micromeritics ASAP-2020 system at liquid nitrogen temperature of −196 °C. Prior to analysis, each sample was degassed at 350 °C for 10 h.

Ammonia temperature-programmed desorption (NH₃-TPD) was carried out in a stainless U-shaped micro-reactor (i.d. = 4 mm). Typically, 0.1400 g sample was loaded in the reactor and pretreated at 605 °C in flowing He with a flowrate of 25 mL min^{−1} for 0.5 h. Then it was cooled down to 150 °C and saturated with NH₃ gas. The reactor temperature was raised from 150 to 605 °C at a heating rate of 19.8 °C min^{−1} and maintained at 605 °C for 0.5 h. The concentration of NH₃ in the exit gas was monitored continuously by a gas chromatograph equipped with a TCD.

Scanning electron microscopy (SEM) was taken using a JSM-7800F field-emission microscope at an acceleration voltage of 30 kV. Transmission electron microscopy (TEM) images were obtained with a JEM-2100 microscope at an acceleration voltage of 200 kV.

Pyridine adsorption-IR (Py-IR) was carried out on a Vertex 70 IR spectrometer (Bruker Corp.). Self-supporting wafers (13 mm diameter) were made from ca. 10 mg zeolite sample and the IR cell can hold the wafer. The pretreatment of the fresh samples was conducted as follows. The cell containing a zeolite wafer was evacuated while slowly increasing the temperature from r.t. to 450 °C and was finally evacuated at 450 °C for 1 h. It was then cooled to r.t. to record the background spectra of zeolite. Infrared spectra were measured at 4 cm^{−1} resolution. After that, the sample was saturated with Py and the excess of Py was removed under vacuum at 150 °C for 0.5 h, after cooling to r.t. it was followed by IR measurements to quantify the amount of total acid sites. Then the excess of Py on the sample was further removed under vacuum at 450 °C for 0.5 h, after cooling to r.t., it was followed by IR measurements to quantify the amount of strong acid sites.

Lewis (AF_L) acid sites. They were initially defined in Ref. [20] and calculated according to Eqs. (1) and (2):

$$AF_B = C_{B-Pn}/C_{B-Py-150} \quad (1)$$

$$AF_L = C_{L-Pn}/C_{L-Py-150} \quad (2)$$

where C_{B-Pn} and C_{L-Pn} represented the concentrations of Brønsted and Lewis acid sites determined by Pn-IR technique respectively, and C_{B-Py-150} and C_{L-Py-150} represented the total concentrations of Brønsted and Lewis acid sites determined by Py-IR technique respectively. All the values were shown in Table 3.

The isotherms of benzene adsorption–desorption were measured on an intelligent gravimetric analyzer (IGA-100) from Hiden Isochema Ltd. This measurement was applied to determine the diffusion properties of the prepared samples, in line with the procedure given in Ref. [26].

2.3 Catalytic Evaluation

The hierarchical zeolite samples were tested in the alkylation of benzene with DME in a stainless fixed bed reactor with 320 mm in length and 12 mm in diameter. All the samples were pressed, crushed and sieved into 0.38–0.85 mm particles before they were loaded into the reactor. 1 g catalyst was located in the middle part of a fixed-bed stainless reactor. Unless specified, the reaction was performed under the conditions of 450 °C, 0.1 MPa, *n*(benzene)/*n*(DME) = 2, and the DME weight hourly space velocity (WHSV) of 8 h^{−1}. Catalyst was activated at 500 °C for 1 h in a nitrogen flow before the reaction. DME and benzene were introduced after the temperature was stable at 450 °C. Both gas and liquid products were collected and analyzed by a GC (Agilent 7890A) equipped with a FID and a PONA capillary column (50 m × 0.2 mm × 0.5 μm). Conversion and selectivity were calculated according to Eqs. (3) and (4):

$$\text{Conversion (\%)} = \frac{\text{Amount of benzene (DME) \% in the feed} - \text{amount of benzene (DME) \% in the products}}{\text{Amount of benzene (DME) \% in the feed}} \times 100 \quad (3)$$

The bands at ca. 1540 cm^{−1} and ca. 1450 cm^{−1} were integrated to determine the concentrations of Brønsted and Lewis acid sites, respectively. In the case of pivalonitile adsorption-IR (Pn-IR), Pn was sorbed at r.t. to determine the amount of acid sites located on external surface, mesopore surface and in pore mouths of the zeolite samples. The accessibility factors (AF) fell into two kinds of factors: the accessibility factors of Brønsted (AF_B) and

$$\text{Selectivity (i) \%} = \frac{\text{Amount of i \% in the products}}{\sum \text{Amount of i \% in the products}} \times 100 \quad (4)$$

where *i* represented one of the gas or liquid products. All the reaction results presented in this work are expressed in weight percent.

3 Results and Discussion

3.1 Characterization of HZSM-11 and Z-*x*at Samples

The XRD patterns (Fig. S1) of all studied zeolites depict the typical diffraction patterns of ZSM-11 zeolite [27]. It has been reported that the C_{NaOH} is found to be the most dominant factor affecting the desilication process [28]. Similarly here, the C_{NaOH} played an important role on the crystallinity of Z-*x*at samples. As the C_{NaOH} increased, the intensity of the XRD peaks decreased progressively. When alkaline treatment was carried out in diluted NaOH solution with C_{NaOH} ranging from 0.1 to 0.3 M, zeolite samples maintained their good crystallinity. However, if the alkaline treatment performed in medium NaOH solution with the C_{NaOH} around 0.5 M, the treated zeolite suffered from partial destruction of its zeolite framework. If the alkaline treatment was done with the more concentrated NaOH solution ranging from 0.6 to 0.7 M, the treated zeolite could be resulted in severe structure destruction. Moreover, when the C_{NaOH} of 1.0 M was used, the framework structure of the treated zeolite was completely collapsed.

The value of relative crystallinity (RC) of Z-*x*at materials are listed in Table 1. The RC value of Z-0.1at increased slightly to 102 %. This could be attributed to the purification by cleaning the amorphous particles on the zeolite surface with diluted NaOH solution [29]. Increasing the C_{NaOH} from 0.2 to 1.0 M, the RC value of the treated zeolites monotonously decreased from 93 to 1 %. Correspondingly, the Si/Al₂ ratios of Z-*x*at zeolites measured by XRF showed a similar tendency and the values monotonously decreased from 53 to 5 (Table 1), obviously due to the essence of alkaline treatment is the rational use of the intrinsic nature of NaOH to selectively remove framework

silicon [28, 30] or more extensive desilication than dealumination in NaOH solution [22, 31].

The isotherms from the N₂ adsorption–desorption measurements of Z-*x*at samples are shown in Fig. 1a, which indicate the changes in the pore structure occurred after the alkaline treatment of the investigated ZSM-11 materials. The total adsorbed amount of N₂ increased and the shapes of the isotherms themselves had changed for the desilicated samples, compared to the pristine zeolite. The HZSM-11 and Z-0.1at samples showed the typical type I isotherm, with a high nitrogen uptake at low relative pressure being characteristic for pure microporous materials. The fabrication of mesopores by treatment of the ZSM-11 zeolite with alkaline medium resulted in a higher adsorption capacity in the range of mesopores. Definitely, the adsorption isotherms for zeolites Z-0.2at to Z-0.7at showed the type I + IV isotherm with enhanced uptake at $P/P_0 = 0.4–1.0$, indicating that there are internal voids with irregular shape between particles with a broad size distribution [32]. The parallel adsorption and desorption branches also verified that there are open and channel-like mesopores for these alkaline treated samples [33]. Moreover, Z-1.0at showed only little N₂ adsorption due to the complete structure collapse. Obviously, the results of N₂ adsorption–desorption measurement were in good agreement with the XRD results.

The BJH pore size distribution (PSD) derived from the N₂ adsorption branches of Z-*x*at is presented in Fig. 1b. The HZSM-11 zeolite showed little mesopore. A kind of broad PSD from 10 to 100 nm could be observed over Z-0.1at, Z-0.2at and Z-0.3at, and the corresponding band intensity increased with the C_{NaOH} . Noticeably, there was a broad band with high intensity centered at ca. 30 nm in the PSDs from Z-0.5at to Z-0.7at samples, indicating that mesopores formed after being treated with NaOH solution.

Table 1 Textural and physiochemical data of HZSM-11 and Z-*x*at samples

Samples	C_{NaOH} (mol L ⁻¹)	Si/Al ₂ ^a	RC ^b	Textural data			
				S_{BET} (m ² g ⁻¹)	S_{ext} (m ² g ⁻¹)	V_{micro} (cm ³ g ⁻¹)	V_{meso} (cm ³ g ⁻¹)
HZSM-11	–	53	100	371	112	0.12	0.30
Z-0.1at	0.1	45	102	427	163	0.12	0.47
Z-0.2at	0.2	36	93	476	224	0.11	0.63
Z-0.3at	0.3	29	70	534	277	0.12	0.88
Z-0.5at	0.5	16	38	503	306	0.09	1.14
Z-0.55at	0.55	15	28	447	271	0.08	1.07
Z-0.6at	0.6	12	19	394	255	0.06	1.01
Z-0.7at	0.7	9	4	330	228	0.04	0.98

^a Si/Al₂: molar ratio detected by XRF

^b RC: relative crystallinity (%)

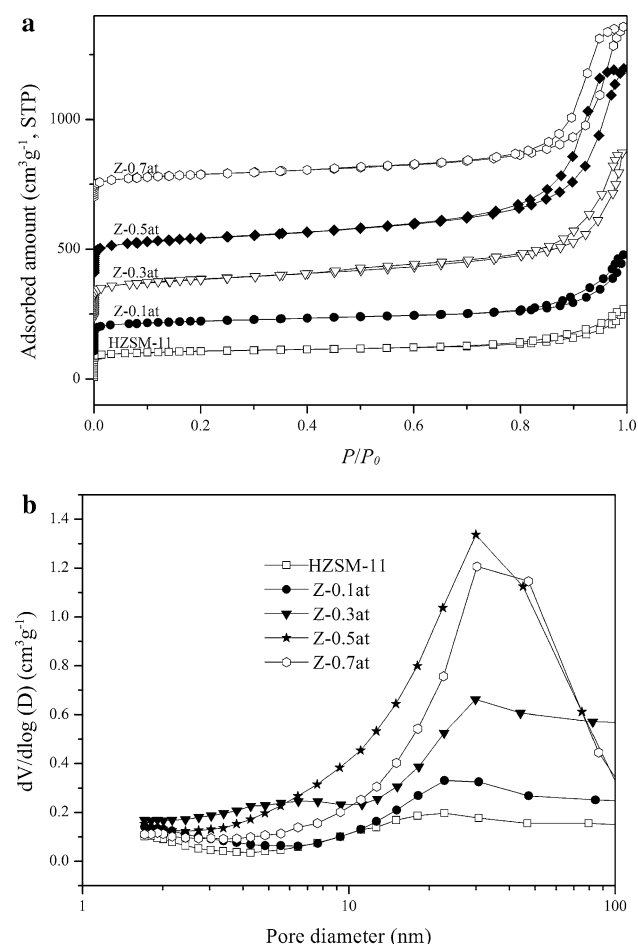


Fig. 1 Nitrogen adsorption–desorption isotherms at $-196\text{ }^{\circ}\text{C}$ (a) and BJH pore size distribution plots derived from the adsorption branch (b) for HZSM-11 and Z-*xat* samples

Besides, the band was in the wide-spread form, which could be attributed to that there were mesopores between particles with a broad size distribution.

The data related N_2 adsorption–desorption isotherms are summarized in Table 1. Obviously, the NaOH treatment could greatly increase both surface area and mesopore volume (V_{meso}). The largest external surface area (S_{ext}) of $306\text{ m}^2\text{ g}^{-1}$ and V_{meso} of $1.14\text{ cm}^3\text{ g}^{-1}$ could be obtained on the Z-0.5at sample. On the other hand, its microporous volume (V_{micro}) decreased by 25 % as compared with the HZSM-11. As reported in Ref. [29], aggravating the severity of the alkaline treatment condition modified the damage of the microporosity and an increase in mesoporosity. The present results also showed that the C_{NaOH} was a crucial factor. If the zeolite was treated with the C_{NaOH} higher than 0.6 M (in the range of 0.6–1.0 M), obvious decrease in both S_{ext} and V_{meso} could be observed, indicating that some part of zeolite structure was collapsed.

IGA technique is a useful tool for characterization of structure properties by applying different adsorbents [34,

35]. As a reactant of the test reaction, benzene molecule was used as the adsorbent in the IGA experiment as reported in our previous work [26]. Here, similar experiment is applied on four typical samples and the results are presented in Fig. S2. The adsorption capacity for the tested samples followed the sequences of Z-0.5at > Z-0.3at > Z-0.1at > HZSM-11, which was in parallel with the variation tendency of S_{ext} and V_{meso} (see Table 1). The results further verified that the diffusion property of ZSM-11 zeolite samples could be greatly improved after being treated with NaOH solution. In general, the higher the capacity of benzene adsorption is, the better the diffusion property of Z-*xat* samples can be [26].

3.2 Morphology Characterization of Z-*xat* Samples

SEM images of Z-*xat* samples are presented in Fig. 2, which reveals the shapes and particle surface of partial material. For HZSM-11 spherical aggregation with particle diameters in a range of 300–400 nm could be observed, and the crystalline grains showed irregular spheroidicity with smooth surface. The sample of Z-0.1at showed similar morphology with the HZSM-11, but the crystalline grains were slightly eroded. In the case of Z-0.3at, this spherical aggregation became loose, and holes appeared on the grains surface. For Z-0.5at, this aggregation almost disappeared, and the grains were significantly destroyed.

TEM images of Z-*xat* samples are also exhibited in Fig. 2. The HZSM-11 showed well-defined micropores. The Z-0.1at sample was similar to the HZSM-11, with no indication of mesopores in crystalline region. In fact, distinct opening pores with wide PSD (10–100 nm) were uniformly distributed in Z-0.3at and Z-0.5at, while the sample Z-0.5at exhibited more loose morphology. These were in accordance with the BJH PSD measurement (Fig. 1b). Such a heavily corrosive surface in Z-0.5at could also be observed over NaOH treated ZSM-5 zeolite [33]. Mesopore production in Z-*xat* was correlated with the cases of ZSM-5 [36] and MOR [37] zeolites. However, the alkaline treated beta zeolite [38] exhibited distinct alteration particularly at the edges of the crystal, contrast to the pore production throughout the whole ZSM-11 zeolite crystal in present work, which may be attributed to the different crystal size. Besides, when ZSM-5 zeolite was leached in NaOH solution under standard conditions (0.2 M, $65\text{ }^{\circ}\text{C}$, 30 min), the TEM images showed mesopores centered ca. 10 nm [39].

3.3 Acidity Characterization of HZSM-11 and Z-*xat* Samples by NH_3 -TPD and FT-IR

The acidities of the HZSM-11 and Z-*xat* materials were investigated by NH_3 -TPD technique. The NH_3 -TPD profile

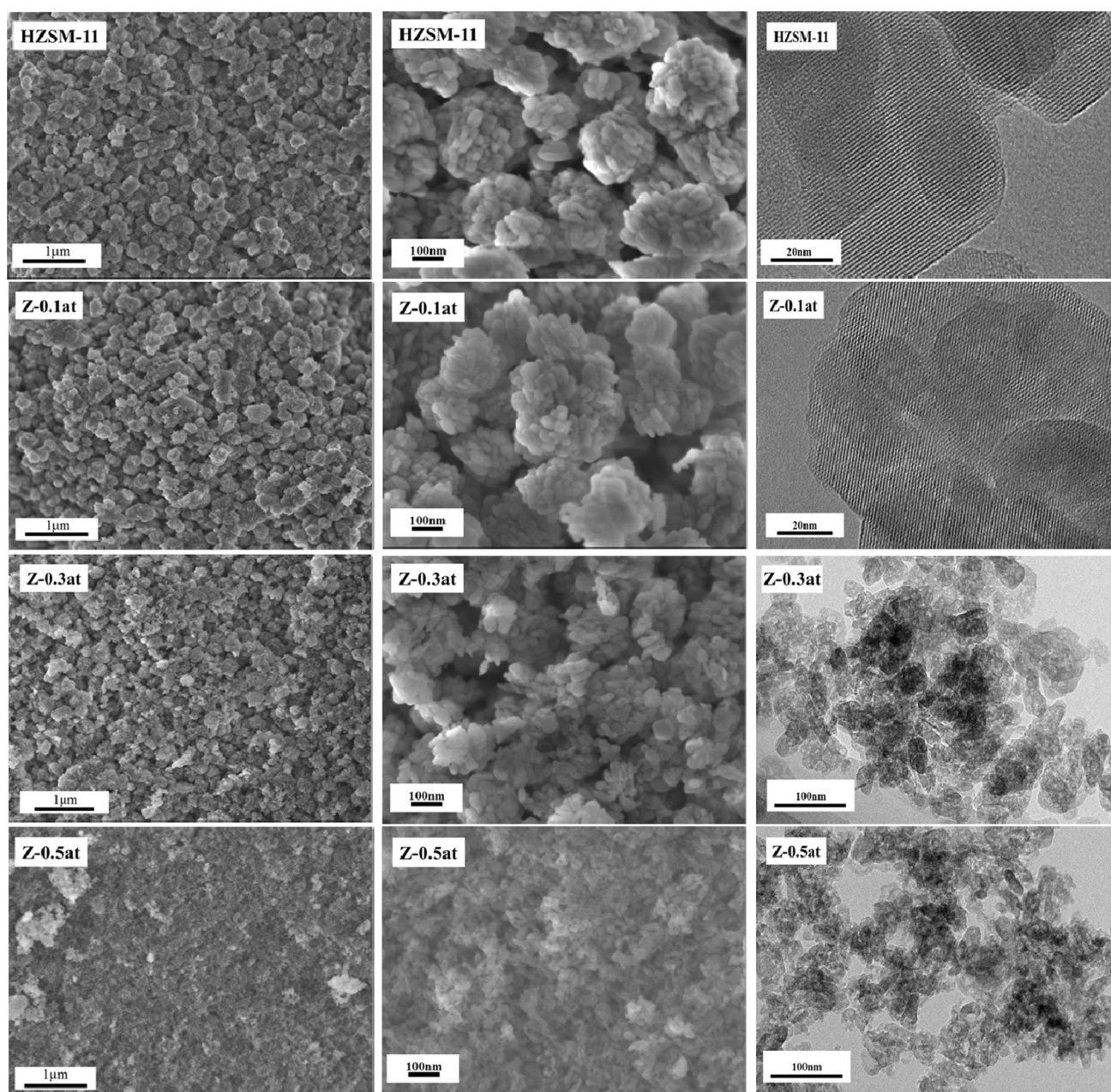


Fig. 2 SEM and TEM images of HZSM-11 and Z-xat samples

of the HZSM-11 sample can be deconvoluted to three desorption bands in the tested temperature range. Typically, the desorption peak temperatures for HZSM-11 are centered at ca. 239, 349 and 440 °C corresponding to the weak, medium and strong acid sites, respectively (Fig. S3a). NH_3 -TPD profiles of HZSM-11 and Z-xat samples and corresponding data obtained from the profiles are presented in Fig. S3b and Table 2, respectively. The total acid concentration (denoted as C_T) of Z-0.1at decreased a little compared with the HZSM-11, which may be attributed to the purification by cleaning the amorphous particles on the zeolite surface with diluted NaOH solution

[29], leading to the significant decrease in weak acid sites. With the increase of C_{NaOH} , the C_T would gradually increase. And the samples of Z-0.5at, Z-0.55at and Z-0.6at showed the highest C_T of ca. 550 $\mu\text{mol g}^{-1}$. If the C_{NaOH} was higher than 0.6 M, due to the partially collapse of zeolite structure, the C_T and strong acid concentration decreased simultaneously.

We should note that except for Z-0.1at and Z-0.7at all the Z-xat samples exhibited a higher C_T compared to the HZSM-11 zeolite, which was in agreement with Groen et al. [10] who reported that zeolite treatment with diluted bases would result in the increasing concentration of acid

sites determined by NH_3 -TPD technique. Besides, since presence of relatively higher Al in the zeolitic framework on account of selective desilication, the C_T increased in alkaline treated samples [28]. Generally, the NH_3 desorption peak temperatures of weak acid sites remained at ca. 240 °C, and those of medium and strong acid sites was ca. 300–320 and ca. 420 °C respectively on Z-*xat* ($x > 0$), which were different from those of the HZSM-11.

The acidities of HZSM-11 and Z-*xat* materials were further investigated by Py-IR technique. The corresponding spectra and results are shown in Fig. S4 and Table 3, respectively. Both the concentrations of the total (Total- P_{y-150}) and strong (Strong- P_{y-450}) acid sites, whether they are Brønsted or Lewis ones, first increased until reaching the highest value on Z-0.3at zeolites and then decreased smoothly from Z-0.3at to Z-0.6at and finally decreased steeply from Z-0.6at to Z-0.7at. Nevertheless, all the Z-*xat* zeolites, except for Z-0.7at, exhibited increased total Brønsted ($C_{B-P_{y-150}}$) and Lewis ($C_{L-P_{y-150}}$) acid concentrations (per gram) compared with the HZSM-11. This was in well agreement with the recent results reported by Sadowska et al. [21, 22], who also reported the notable increase in concentrations of Brønsted and Lewis acid sites, while contracted with the results reported by Milina et al. [16].

The ratio of total Brønsted to Lewis acid concentration ($B/L_{-P_{y-150}}$) of the HZSM-11 was 1.42. While Z-0.1at sample showed a reduced $B/L_{-P_{y-150}}$ value of 1.32. When HZSM-11 zeolite was treated with a more concentrated NaOH solution, Z-*xat* (x is in the range of 0.2–0.7) materials would present a similar $B/L_{-P_{y-150}}$ value of ca. 1.00, which was inconsistent with previous reports [16, 22, 31].

While the ratio of strong Brønsted to Lewis acid concentration ($B/L_{-P_{y-450}}$) on HZSM-11 and Z-*xat* samples decreased faster than $B/L_{-P_{y-150}}$ with the increase of C_{NaOH} . For HZSM-11 the $B/L_{-P_{y-450}}$ value was 4.63, which was significantly higher than those of Z-*xat* samples, and the value decreased monotonously from 2.65 to 0.77 with C_{NaOH} . In the case of the weak-medium acid concentration ($WM_{-P_{y-150-450}}$), it first increased and then decreased, reaching the highest value at C_{NaOH} of 0.5 M. Meanwhile, the ratio of weak-medium Brønsted to Lewis acid concentration ($B/L_{-P_{y-WM}}$) of Z-*xat* increased from 0.16 to 1.48 when the C_{NaOH} increased from 0 to 0.6 M.

In summary, alkaline treatment resulted in the decrease in Strong- P_{y-450} and the increase $WM_{-P_{y-150-450}}$, which was in well agreement with the results reported in Ref. [36]. Besides, the acid sites distributions ($B/L_{-P_{y-150}}$, $B/L_{-P_{y-450}}$ and $B/L_{-P_{y-WM}}$) showed different tendency with C_{NaOH} .

It should be noticed that the resultant acidities of HZSM-11 and Z-*xat* materials obtained by Py-IR technique showed some differences from those obtained by NH_3 -TPD (Table 2). The total acid concentrations of the tested

Table 2 Characterization results of HZSM-11 and Z-*xat* zeolites by NH_3 -TPD technique

Samples	Concentration of acid sites ($\mu\text{mol g}^{-1}$)			
	Total	Weak	Medium	Strong
HZSM-11	466	138 (240) ^a	94 (349)	234 (440)
Z-0.1at	448	107 (232)	97 (302)	244 (423)
Z-0.2at	468	118 (238)	104 (300)	246 (421)
Z-0.3at	530	140 (240)	122 (302)	268 (420)
Z-0.5at	543	159 (244)	205 (310)	179 (423)
Z-0.55at	547	174 (240)	189 (312)	184 (422)
Z-0.6at	549	184 (244)	175 (320)	190 (428)
Z-0.7at	460	161 (244)	163 (320)	136 (424)

^a Data presented in parentheses were the desorption peak temperatures (°C) of NH_3 -TPD profiles

samples obtained by Py-IR technique (Table 3) were lower compared to that determined by TPD of NH_3 (Table 2). The possible reason is that part of the acid sites is inaccessible to bulky pyridine molecules but can be reached by NH_3 molecules [18, 40, 41], or that the possible formation of $\text{NH}_4^+n\text{NH}_3$ association [42] during NH_3 -TPD measurement leads to a higher acid concentration.

IR technique of Pn adsorption (Pn-IR) was applied to determine both the Brønsted and the Lewis acid sites situated on external surfaces and in pore mouths (hereafter collectively called external surface) of HZSM-11 and hierarchical Z-*xat* materials, which followed the Ref. [20]. The normalized and deconvoluted spectrum of Pn-IR on the Z-0.5at sample (Fig. 3a) showed three bands centered at 2248, 2277, and 2305 cm^{-1} , respectively, which were well consistent with the results reported in Ref. [20]. Pn-IR spectra of HZSM-11 and Z-*xat* samples are shown in Fig. 3b. The corresponding Brønsted (C_{B-P_n}) and Lewis (C_{L-P_n}) acid concentrations listed in Table 3 were calculated based on the extinction coefficients following the Ref. [20].

The HZSM-11 zeolite contained little acid sites accessible to hindered Pn molecules (1 $\mu\text{mol g}^{-1}$ for C_{B-P_n} and 5 $\mu\text{mol g}^{-1}$ for C_{L-P_n} , respectively). Both the C_{B-P_n} and C_{L-P_n} of the Z-*xat* materials first increased and then decreased with the C_{NaOH} , and the sample of Z-0.3at exhibited the highest value (180 $\mu\text{mol g}^{-1}$ for C_{B-P_n} and 34 $\mu\text{mol g}^{-1}$ for C_{L-P_n} , respectively) among the tested samples. Moreover, the B/L ratios determined by Pn-IR (B/L_{-P_n}) of all the Z-*xat* samples ($x > 0$) were remarkably higher than that of the HZSM-11, implying that there was an obvious change in external acid sites distribution after treatment with NaOH solution. Besides, for all Z-*xat* ($x > 0$) samples, the B/L_{-P_n} value was higher than the corresponding $B/L_{-P_{y-150}}$ value, indicating that after the alkaline treatment the distribution and concentrations of

Table 3 Characterization results of HZSM-11 and Z-xat zeolites by FT-IR techniques

Samples	Concentration of acid sites ($\mu\text{mol g}^{-1}$)											
	Determined with pyridine									Determined with pivalonitrile ^f		
	Total ^a _{Py-150}			WM ^d _{Py-150-450}			Strong ^e _{Py-450}			C_{B-Pn}	C_{L-Pn}	B/L- Pn
	$C_{B-Py-150}^b$	$C_{L-Py-150}^c$	B/L- $Py-150$	$C_{B-Py-WM}$	$C_{L-Py-WM}$	B/L- $Py-WM$	$C_{B-Py-450}$	$C_{L-Py-450}$	B/L- $Py-450$			
HZSM-11	151	106	1.42	12	76	0.16	139	30	4.63	1	5	0.2
Z-0.1at	173	131	1.32	51	85	0.60	122	46	2.65	90	16	5.6
Z-0.2at	157	136	1.15	53	85	0.62	104	51	2.04	106	30	3.5
Z-0.3at	236	214	1.10	81	102	0.79	155	112	1.38	180	34	5.2
Z-0.5at	190	202	0.94	95	106	0.90	95	96	0.99	98	23	4.3
Z-0.55at	177	176	1.01	97	90	1.08	80	86	0.93	–	–	
Z-0.6at	178	153	1.16	99	67	1.47	79	86	0.92	69	16	4.3
Z-0.7at	92	93	0.99	59	50	1.18	33	43	0.77	–	–	

^a Total_{Py-150}: total acid concentration determined by Py-IR technique at 150 °C

^b C_B : Brønsted acid concentration

^c C_L : Lewis acid concentration

^d WM_{Py-150-450}: weak-medium acid concentration was defined as the difference between the total and strong acid concentration

^e Strong_{Py-450}: strong acid concentration determined by Py-IR technique at 450 °C

^f The extinction coefficients of the IR bands of pivalonitrile interacting with both Brønsted ($0.11 \text{ cm}^2 \mu\text{mol}^{-1}$) and Lewis ($0.16 \text{ cm}^2 \mu\text{mol}^{-1}$) acid sites were reported in Ref. [20]

acid sites on the external surface of Z-xat were quite different from that in the bulk.

The diagrams representing the dependence of AF_B and AF_L of the HZSM-11 and Z-xat samples on the C_{NaOH} are presented in Fig. 4. For all samples, the value of AF_B was higher than that of AF_L on the whole. The HZSM-11 zeolite contained little Brønsted and Lewis acid sites accessible to Pn molecules, leading to the small AF_B value of 0.6 % and AF_L value of 4.7 %. For the Z-xat zeolites, with the increase of C_{NaOH} , both the AF_B and AF_L values first increased and then decreased. Besides, when C_{NaOH} was less than 0.5 M, the AF values basically correlated with S_{ext} and V_{meso} of materials since their crystallinities were preserved well. However, for the materials treated in concentrated NaOH solution (0.5–1.0 M), the AF values did not correlate with the S_{ext} and V_{meso} , somehow different from the results reported in Ref. [20]. This may be because that the resultant materials treated in more concentrated NaOH solution are partially amorphous, which changes the concentration and distribution of acid sites over the zeolites.

3.4 Reaction Performance

The reaction performance of alkylation of benzene with DME on HZSM-11 and Z-xat zeolite catalysts were investigated. Since the similar zeolite topology results in similar product distribution [43], almost the same product distributions can be obtained on HZSM-11 and Z-xat

zeolite catalysts. Here, we take Z-0.5at zeolite catalyst as an example (Fig. 5). The initial conversions (the conversions at the reaction time on stream (TOS) of 2 h) of benzene and DME were ca. 48 and 100 %, respectively. Besides, their variation with TOS is shown in Figs. 6a, b. During the 73 h TOS, the selectivities of dry gas (<1 %) and LPG (<2 %) over Z-0.5at were still very low, and the selectivity of the liquid products was as high as ca. 97 %.

As shown in Fig. 5, when running for the 73 h, the selectivity of toluene increased from 46 to 62 %. The selectivities of xylene and trimethylbenzene first kept constant (in TOS range of 0–58 h) and then decreased. In the case of C_{5-6} , the selectivity first increased a little and then decreased slowly. Meanwhile the selectivities of ethylbenzene, propylbenzene and ethyltoluene decreased with TOS.

Based on the above results, a possible reaction route is illustrated in Scheme S1. Firstly, a proton from the zeolite attacked DME to form methyl and methoxy species [25]. A methoxy cation then attacked a benzene molecule to form toluene. The xylene and trimethylbenzene formed in the similar manner: a methoxy cation attacked a toluene or xylene. Therein, the toluene and xylene were the main liquid products, similar to the case of ZSM-5 [25]. On the other hand, DME could be converted to hydrocarbones (C_xH_y) and aromatics after being activated [44]. Also the formed C_xH_y could be activated and then attacked benzene or other aromatic molecules to produce alkyl-aromatics, such as ethylbenzene, propylbenzene and ethyltoluene,

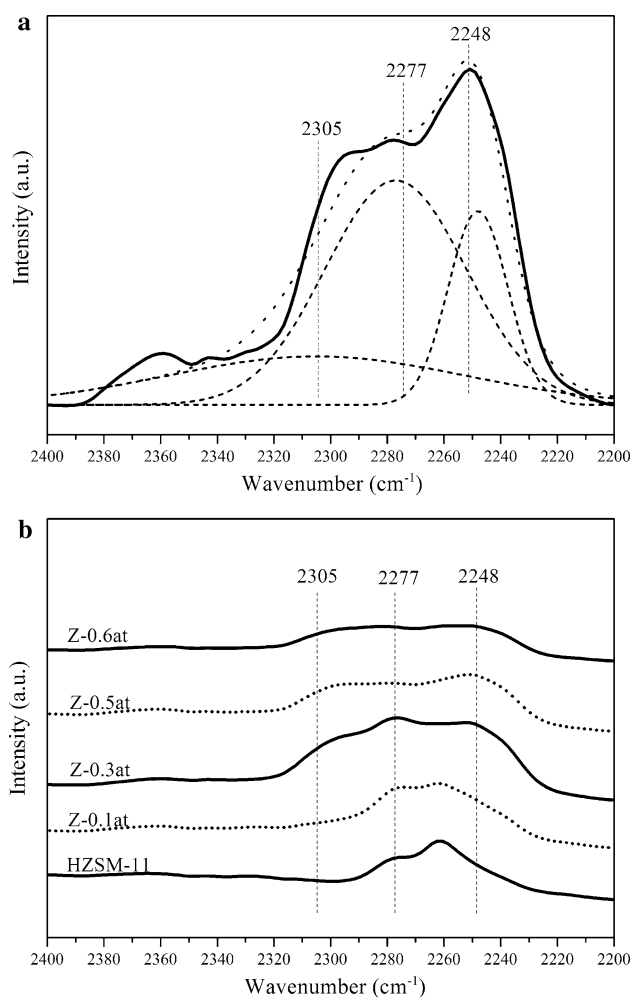


Fig. 3 Pn-IR spectra recorded at r.t. on Z-0.5at sample (a) and HZSM-11 and Z-*x*at samples (b)

although these products took only a small part. With the reaction progress, the specific selectivities of products would vary with TOS as shown in Fig. 5.

As reported in Ref. [45], the NaOH treatment of the parent zeolite causes the main effect on the stability in the conversion of methanol. Similarly in our present study, the alkylation stability of benzene with DME over HZSM-11 and Z-*x*at zeolite catalysts is compared and the results are shown in Fig. 6 (a, based on DME conversion; b, based on benzene conversion). The scattering of benzene conversion data is very likely due to the fluctuation in the evaporation of benzene [25]. Except for Z-1.0at with much poor reaction performance, the initial DME conversion of 100 % and initial benzene conversion of ca. 48 % were similar for all Z-*x*at zeolite catalysts. When the conversion of benzene began to decrease, the ratio of DME conversion to benzene conversion became higher and higher with the reaction progress, suggesting the reactivity of DME is higher than that of benzene in the feed. As expected, the HZSM-11

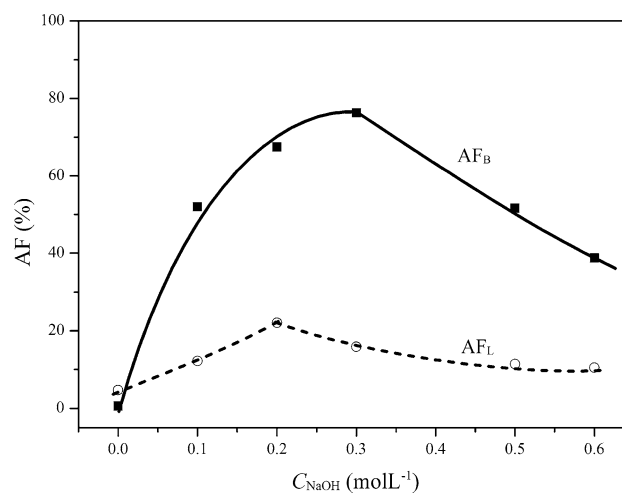


Fig. 4 Plots of AF_B and AF_L versus alkaline concentration

zeolite with pure micropores exhibited a dramatic decay in conversions of benzene and DME after 12 h on stream. The stability of Z-*x*at catalysts first increased and then decreased with the increase of C_{NaOH} . Therein, Z-0.5at zeolite catalyst showed the best performance, which maintained its stable conversion for ca. 50 h.

3.5 Relevance of Reaction Stability and Porosity as Well as Acidity of HZSM-11 and Z-*x*at Catalysts

Although the initial DME and benzene conversions were similar for all the investigated ZSM-11 catalysts, their reaction stabilities showed remarkable difference. For convenience, two indexes are used to measure the reaction stability: one is T_D which is defined as the TOS when the DME conversion decreased to 95 %, and the other is T_B which means the TOS when the benzene conversion decreased to 34 %.

The influences of the textural properties and acidities over HZSM-11 and Z-*x*at catalysts on the reaction stability of alkylation of benzene with DME were further investigated. As shown in Fig. 7, it was interesting to notice that the change of V_{meso} was in line with that of reaction stability. Increasing C_{NaOH} from 0 to 0.5 M, the V_{meso} and the reaction stability increased together. With C_{NaOH} further increasing to 0.7 M, the V_{meso} and the stability decreased consistently. Therein, Z-0.5at showed the highest V_{meso} and the best stability with T_D of 57 h and T_B of 64 h. This could be attributed to the better diffusion capability of the catalyst caused by the generation of open mesopores, which facilitated the diffusion of coke precursors [9]. The V_{micro} first maintained at ca. $0.12 \text{ cm}^3 \text{ g}^{-1}$ and then decreased with C_{NaOH} , while the V_{meso} first increased and then decreased. For Z-0.5at the former was $0.09 \text{ cm}^3 \text{ g}^{-1}$

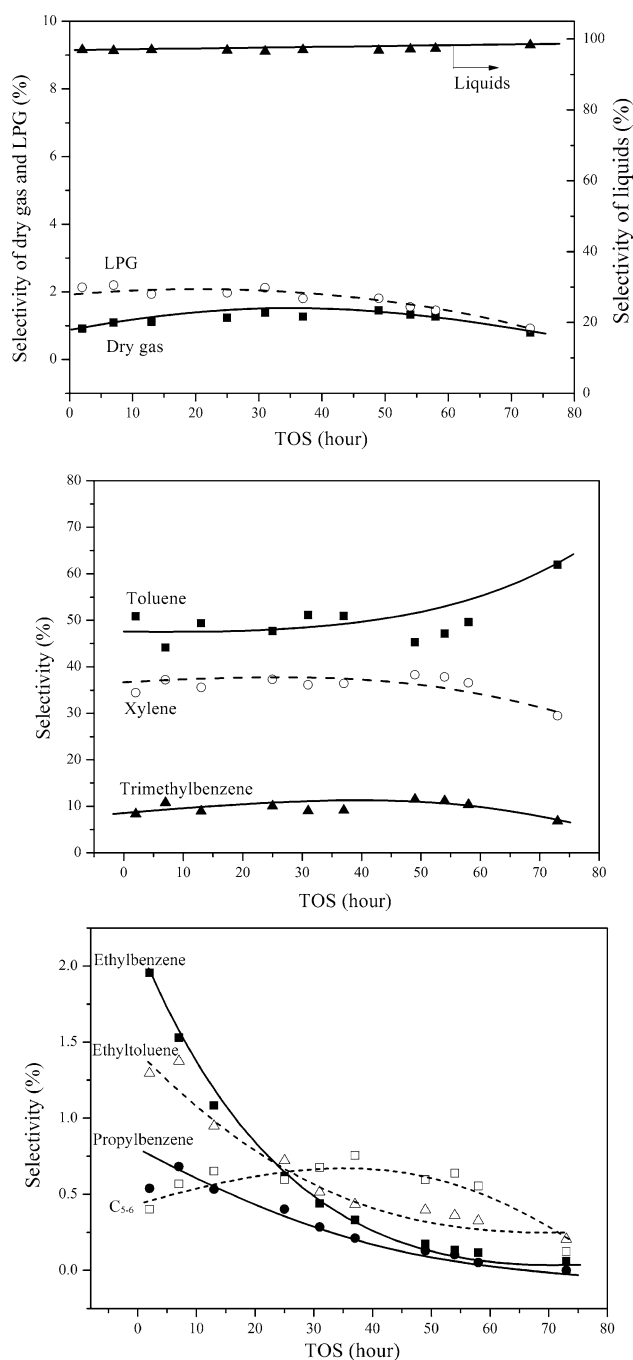


Fig. 5 Products selectivities as a function of TOS over Z-0.5at

and the latter was $1.14 \text{ cm}^3 \text{ g}^{-1}$. Therefore, the suitable balance between mesoporosity and microporosity is the essential factor to improve the stability [8].

In the case of the NaOH treated ZSM-11 materials the additional porosity was not the only reason for the improved reaction stability. As reported by Refs. [9, 12, 36, 46], the changes in both acidic properties and porosity influenced the catalytic properties of the catalysts, nevertheless the authors did not analyze specifically the

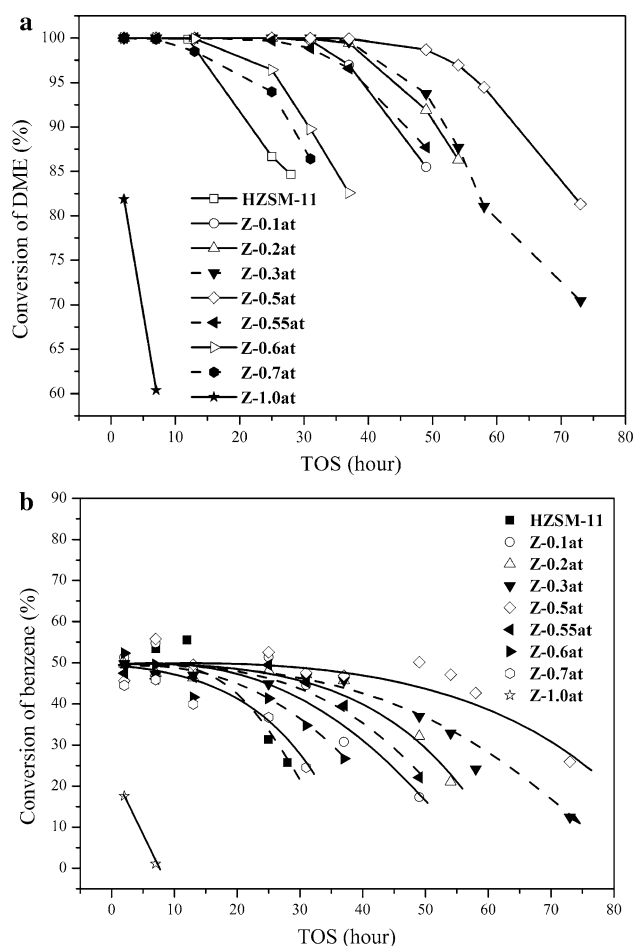


Fig. 6 Reaction stability of HZSM-11 and Z-xat zeolite catalysts

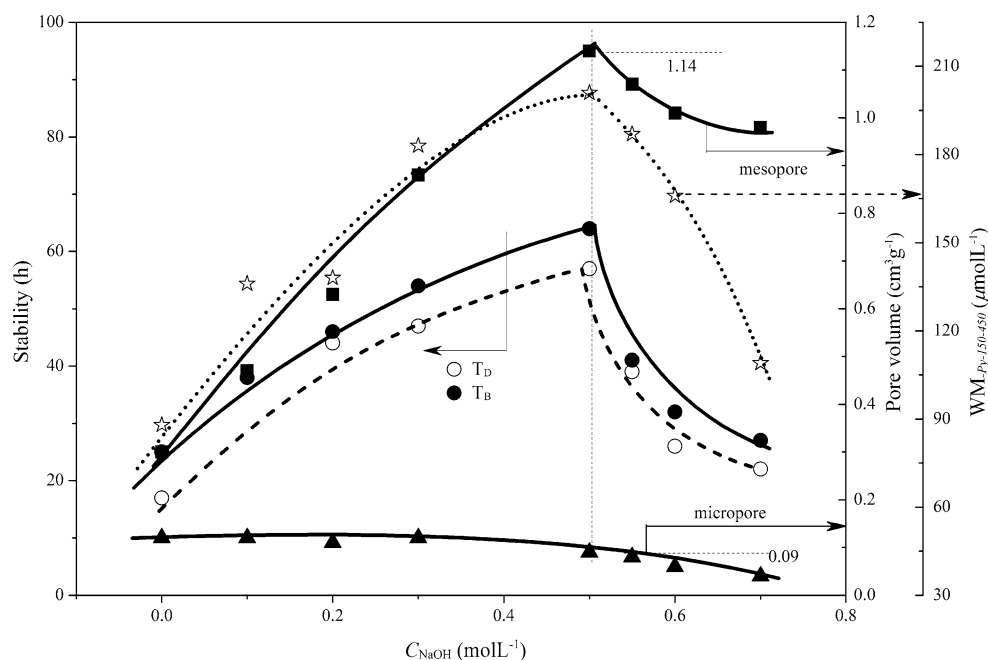
correlation between these two parameters with catalytic performance.

To evaluate the influence of acidity on reaction performance, NH_3 -TPD, Py-IR and Pn-IR techniques were applied as well. In Sect. 3.3, we described and discussed the properties of acidity, including their concentration, intensity, distribution (B/L-Py-150 , B/L-Py-450 , B/L-Py-WM and B/L-Pn) and AF. Relating these properties with the reaction stability, it was interesting to find that the WM-Py-150-450 was well accordant with the stability (Fig. 7).

As shown in Fig. 7, the mesoporosity was positively related to the reaction stability. Generally speaking, coke deposition is the reason for zeolite catalyst deactivation [47]. The origin of superior stability can be explained in terms of the facile diffusion of coke precursors from the micropores to the surfaces of the mesopore walls owing to the large external surface area and the short diffusion path length [9]. It should be noticed that we did not investigate the coke of the used samples in present work.

The reaction stability can be promoted by reducing the number of strong acid sites and meanwhile increasing the

Fig. 7 Variation of stability, pore volumes and $WM_{Py-150-450}$ with C_{NaOH} of HZSM-11 and Z-xat catalysts



mesoporosity [9]. As shown in Table 3, $C_{B-Py-450}$ of Z-xat samples were lower than the HZSM-11 on the whole, therefore, the decreased $C_{B-Py-450}$ may be beneficial to the improved reaction stability. However these two parameters did not show clear linear relation.

DME-to-olefins reaction is favored by the weak acidity because the Brønsted acid sites have the ability to bind the methoxy species, and the weak acid intensities are beneficial to reduce hydrogen transfer reaction rate, then to lower the formation rate of coke and heavy hydrocarbons [48, 49]. Besides, the weak acid site is responsible for the reaction of aromatization, whereas the strong acid center is more likely to be the deactivation center in the methanol aromatization reaction over ZSM-5 zeolite [50]. It was also reported that from the NH_3 -TPD profile of the deactivated hierarchical zeolite, the strong acid sites, which are responsible for catalyzing the MTH reaction, are not available for NH_3 adsorption anymore. While a large number of weak acid sites are still able to adsorb NH_3 [51]. Similarly in our present work, the strong acid sites were poisoned by the deposition of coke soon after the beginning of the reaction, and the remaining weak-medium acid sites turned to be the major active centers. This may be the reason that the $WM_{Py-150-450}$ could be positively related with the reaction stability (Fig. 7).

It was believed that during NaOH treatment of ZSM-5 zeolite some protonic sites situated on amorphous silica-alumina material were of weaker acid strength than typical zeolitic Si-OH-Al groups (strong acid sites) [24]. This was similar with the case of weak-medium acid sites in our present work. The changes in the $WM_{Py-150-450}$ with

C_{NaOH} could be attributed to the formation of mesopores. Most likely, these acid sites or these amorphous silica-alumina materials were mainly situated on the mesopores, leading to the consistence of $WM_{Py-150-450}$ with V_{meso} . Therefore, the reaction stability of the studied zeolites depended on the combination of $WM_{Py-150-450}$ with V_{meso} (Fig. 7).

4 Conclusion

ZSM-11 zeolite has been modified with NaOH, resulting in a series of samples (Z-xat) with different porosity and acidity. Textural properties for ZSM-11 zeolite showed that at an appropriate NaOH concentration, external surface area and mesopore volume were found to be observably improved.

Acidic properties of the alkaline treated samples were investigated in detail. NH_3 -TPD measurement revealed that the total acid concentrations of Z-xat increased as a whole compared with the HZSM-11 except for Z-0.1at and Z-0.7at, and the value first increased and then decreased with C_{NaOH} . Py-IR technique showed that with the increase of C_{NaOH} , the ratio of total Brønsted to Lewis acid concentration of Z-xat first decreased a little and then kept around 1.00, while that of the strong Brønsted to Lewis acid concentration reduced regularly. IR technique of pivalonitrile adsorption indicated that NaOH treatment changed the B/L value on the external surface and this value was of obvious difference from that in the bulk. The AF of acid sites for Z-xat samples revealed that the AF_B

was higher than the AF_L as a whole, besides the evolution of both values with C_{NaOH} showed similar regulation.

The reaction stability of alkylation of benzene with DME over the HZSM-11 and Z-rat zeolite catalysts was closely linked with both porosity and acidity. The superior reaction stability of the alkaline treated ZSM-11 zeolite catalysts resulted from the interplay of the improved diffusion property by mesoporosity and appropriate weak-medium acidity determined by Py-IR technique.

Acknowledgments The guidance and help of Professor Yide Xu is greatly appreciated.

References

- Zhang L, Liu HJ, Li XJ, Xie SJ, Wang YZ, Xin WJ, Liu SL, Xu LY (2010) *Fuel Process Technol* 91:449
- Xie PF, Ma Z, Zhou HB, Huang CY, Yue YH, Shen W, Xu HL, Hua WM, Gao Z (2014) *Microporous Mesoporous Mater* 191:112
- Liu H, Wei HJ, Xin WJ, Liu SL, Xie SJ, Xu LY (2014) *Acta Pet Sin (Pet Process)* 30:115
- Jury FA, Polaert I, Estel L, Pierella LB (2014) *Microporous Mesoporous Mater* 198:22
- Derouane EG, Andre J-M, Lucas AA (1988) *J Catal* 110:58
- Perez-Ramirez J, Christensen CH, Egeblad K, Christensen CH, Groen JC (2008) *Chem Soc Rev* 37:2530
- Verboekend D, Pérez-Ramírez J (2011) *Catal Sci Technol* 1:879
- Li YN, Liu SL, Zhang ZK, Xie SJ, Zhu XX, Xu LY (2008) *Appl Catal A Gen* 338:100
- Kim J, Choi M, Ryoo R (2010) *J Catal* 269:219
- Groen JC, Moulijn JA, Pérez-Ramírez J (2005) *Microporous Mesoporous Mater* 87:153
- Wang LY, Wang Y, Wang AJ, Li X, Zhou F, Hu YK (2013) *Microporous Mesoporous Mater* 180:242
- Schmidt F, Lohe MR, Büchner B, Giordanino F, Bonino F, Kaskel S (2013) *Microporous Mesoporous Mater* 165:148
- Liu J, Zhang C, Shen Z, Hua W, Tang Y, Shen W, Yue Y, Xu H (2009) *Catal Commun* 10:1506
- Thibault-Starzyk F, Stan I, Abelló S, Bonilla A, Thomas K, Fernandez C, Gilson J-P, Pérez-Ramírez J (2009) *J Catal* 264:11
- Nesterenko NS, Thibault-Starzyk F, Montouillout V, Yushchenko VV, Fernandez C, Gilson JP, Fajula F, Ivanova II (2006) *Kinet Catal* 47:40
- Milina M, Mitchell S, Michels N-L, Kenvin J, Perez-Ramirez J (2013) *J Catal* 308:398
- Góra-Marek K, Tarach K, Choi M (2014) *J Phys Chem C* 118:12266
- Góra-Marek K, Tarach K, Tekla J, Olejniczak Z, Kuśtrowski P, Liu L, Martinez-Triguero J, Rey F (2014) *J Phys Chem C* 118:28043
- Holm MS, Svelle S, Joensen F, Beato P, Christensen CH, Bordiga S, Bjørgen M (2009) *Appl Catal A Gen* 356:23
- Sadowska K, Góra-Marek K, Datka J (2013) *J Phys Chem C* 117:9237
- Sadowska K, Góra-Marek K, Datka J (2012) *Vib Spectrosc* 63:418
- Sadowska K, Góra-Marek K, Drozdek M, Kuśtrowski P, Datka J, Triguero JM, Rey F (2013) *Microporous Mesoporous Mater* 168:195
- Rac V, Rakić V, Stošić D, Otman O, Auroux A (2014) *Microporous Mesoporous Mater* 194:126
- Gil B, Mokrzycki Ł, Sulikowski B, Olejniczak Z, Walas S (2010) *Catal Today* 152:24
- Széchenyi A, Solymosi F (2008) *Catal Lett* 127:13
- Liu H, Wei HJ, Xin WJ, Song C, Xie SJ, Liu ZN, Liu SL, Xu LY (2014) *J Energy Chem* 23:617
- Yu QJ, Chen J, Zhang Q, Li CY, Cui QK (2014) *Mater Lett* 120:97
- Wei XT, Smirniotis PG (2006) *Microporous Mesoporous Mater* 97:97
- Liu KF, Xie SJ, Xu GL, Li YN, Liu SL, Xu LY (2010) *Appl Catal A Gen* 383:102
- Qin ZX, Shen BJ, Gao XH, Lin F, Wang BJ, Xu CM (2011) *J Catal* 278:266
- Sadowska K, Wach A, Olejniczak Z, Kuśtrowski P, Datka J (2013) *Microporous Mesoporous Mater* 167:82
- Kruk M, Jaroniec M (2001) *Chem Mater* 13:3169
- Milina M, Mitchell S, Crivelli P, Cooke D, Pérez-Ramírez J (2014) *Nature Commun*. doi:10.1038/ncomms4922
- Zhao L, Shen BJ, Gao JS, Xu CM (2008) *J Catal* 258:228
- Yue YY, Liu HY, Yuan P, Li TS, Yu CZ, Bi H, Bao XJ (2014) *J Catal* 319:200
- Svelle S, Sommer L, Barbera K, Vennestrøm PNR, Olsbye U, Lillerud KP, Bordiga S, Pan Y-H, Beato P (2011) *Catal Today* 168:38
- Ordonsky VV, Ivanova II, Knyazeva EE, Yuschenko VV, Zai-kovskii VI (2012) *J Catal* 295:207
- Groen JC, Abelló S, Villaescusa LA, Pérez-Ramírez J (2008) *Microporous Mesoporous Mater* 114:93
- Perez-Ramirez J, Verboekend D, Bonilla A, Abello S (2009) *Adv Funct Mater* 19:3972
- Awayssa O, Al-Yassir N, Aitani A, Al-Khattaf S (2014) *Appl Catal A Gen* 477:172
- Góra-Marek K, Derewiński M, Sarv P, Datka J (2005) *Catal Today* 101:131
- Lónyi F, Valyon J (2001) *Microporous Mesoporous Mater* 47:293
- Jae J, Tompsett GA, Foster AJ, Hammond KD, Auerbach SM, Lobo RF, Huber GW (2011) *J Catal* 279:257
- Keckemeti A, Barthos R, Solymosi F (2008) *J Catal* 258:111
- Lietz G, Schnabel KH, Peuker C, Gross T, Storek W, Volter J (1994) *J Catal* 148:562
- Bjørgen M, Joensen F, Holm MS, Olsbye U, Lillerud K-P, Svelle S (2008) *Appl Catal A Gen* 345:43
- Mei CS, Wen PY, Liu ZC, Liu HX, Wang YD, Yang WM, Xie ZK, Hua WM, Gao Z (2008) *J Catal* 258:243
- Zhao TS, Takemoto T, Tsubaki N (2006) *Catal Commun* 7:647
- Ahmed MHM, Muraza O, Al Amer AM, Sugiura Y, Nishiyama N (2015) *Microporous Mesoporous Mater* 207:9
- Yang FK, Wang SM, Xia YM, Bi WH, Wang W (2011) *Pet Sci Technol* 29:1675
- Schmidt F, Hoffmann C, Giordanino F, Bordiga S, Simon P, Carrillo-Cabrera W, Kaskel S (2013) *J Catal* 307:238